Available online at www.sciencedirect.com
ScienceDirect
Dyes and Pigments 79 (2008) 183–192
DYES and PIGMENTS
www.elsevier.com/locate/dyepig

Polymorph prediction of organic pigments

N. Panina [a], R. van de Ven [a], P. Verwer [b], H. Meekes [a,*], E. Vlieg [a], G. Deroover [c]

[a] IMM Solid State Chemistry, Radboud University Nijmegen, Toernooiveld 1, 6525 ED Nijmegen, The Netherlands
[b] Akzo Nobel Chemicals B.V., Department of CPT, P.O. Box 9300, 6800 SB Arnhem, The Netherlands
[c] Agfa-Gevaert N.V., Septestraat 27, B-2640 Mortsel, Belgium

Received 19 February 2007; received in revised form 13 February 2008; accepted 14 February 2008
Available online 26 February 2008

Abstract

The crystal structure of several industrially important organic pigments namely C.I. Pigment Violet 23, C.I. Pigment Red 202 and C.I. Pigment Yellow 139 were predicted using the Cerius^2 Polymorph Predictor in combination with XRPD patterns. After generation and energy minimisation of the candidate structures for each pigment, their calculated powder patterns were compared with those obtained experimentally using X-ray diffraction. The structures which best fitted the experimental powder patterns were regarded as possible structures of the compound; finally, a rigid body Rietveld refinement was performed to validate the choice of the structure. The structure of C.I. Pigment Violet 23 has not previously been published while the predicted structures of C.I. Pigment Red 202 and C.I. Pigment Yellow 139 were in accordance with the published structures. The work demonstrates that pigment crystal structure can be predicted using a low quality X-ray powder diffraction pattern.

Keywords: Polymorph; Crystal structure prediction; PV23; PR202; PY139; X-ray powder diffraction

1. Introduction

Pigments are organic or inorganic colorants that are used in the form of insoluble powders. Today, the use of pigments is widespread and includes coating technology, paints, inks and plastic coloration as well as relatively new technologies such as information storage systems [1].

The color of a pigment depends strongly on the structure and morphology of the crystalline particles. Therefore, to fully understand and be able to control the color properties of a pigment it is vital to know its crystal structure. However, since an essential property of a high quality pigment is its small particle size and insolubility, traditional approaches to obtaining crystal structures are not always successful. On the one hand, routine solution growth is in most cases impossible due to the intrinsic low solubility, although exceptions are known [2], while vapour growth, if successful, rarely results in crystals of sufficient quality or size. Therefore, single crystal X-ray diffraction in most cases cannot be used for the structure determination. On the other hand, small crystallite sizes usually cause considerable broadening and overlapping of the peaks in the X-ray powder diffraction (XRPD) pattern making the indexing and further structure determination very difficult, despite the usual rigidity of the molecules.

An alternative method is to determine the crystal structure using lattice energy minimisation methods, also known as crystal structure prediction (CSP). CSP is used to predict all possible polymorphs of a certain compound starting from the molecular structure. Several blind tests organised recently by the Cambridge Crystallographic Data Centre [3–5] illustrate the state-of-the-art in this area and have shown the best results in case of rigid molecules compared to flexible molecules. Although CSP has not become a routine technique on its own yet, it is considered to be a helpful tool in searching for new polymorphs. Especially, when applied to rigid molecules and combined with experimental techniques like XRPD the predictive power is quite promising [6–8].

Here, we study the predictive power of the method using the Polymorph Predictor combined with XRPD data for three different pigments, C.I. Pigment Violet 23, C.I. Pigment Red 202 and C.I. Pigment Yellow 139 (Fig. 1).

* Corresponding author. Tel.: +31 24 3653200; fax: +31 24 3653067.
E-mail address: hugo.meekes@science.ru.nl (H. Meekes).

0143-7208/$ - see front matter © 2008 Elsevier Ltd. All rights reserved.
doi:10.1016/j.dyepig.2008.02.006

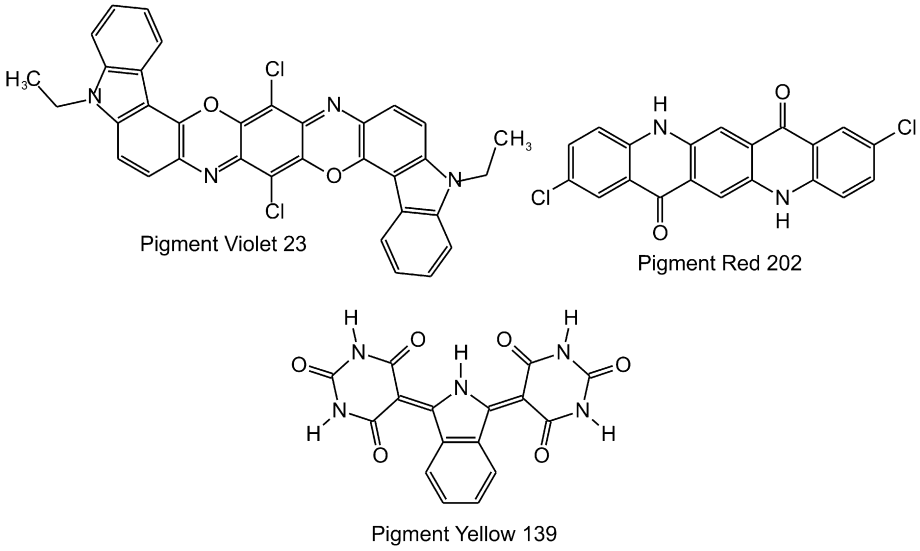

Fig. 1. Pigment Violet 23, Pigment Red 202 and Pigment Yellow 139.

2. Crystal structure prediction

Crystal structure prediction was performed using the Polymorph Predictor (PP) module in Cerius^2 [9]. The molecules of the pigments were first drawn and energetically optimised in the Dreiding 2.21 force field. Electrostatic potential derived (ESPD) atomic point charges were obtained from ab initio Hartree–Fock calculations on the optimised molecule using Gaussian [10] with the 6-31G(d) basis set. The energy of the molecule was then minimised again with the atomic charges in the Dreiding 2.21 force field and the result was used as input for the PP. The same force field with Ewald summation for the Van der Waals and electrostatic interactions was used in the PP for the calculation and minimisation of energy. Default settings for the PP procedure were used unless otherwise specified. For further details the reader is referred to Refs. [9,8].

For evaluation of the prediction results, X-ray powder diffraction patterns of all pigments were obtained using a Philips PW 1710 diffractometer with Cu Kα radiation of wavelength 1.5418 Å by scanning the samples over 2θ angles ranging from 2° to 50°. Rigid body Rietveld refinement was performed using the program DBWS-9006 [11] interfaced from Cerius^2. The refinement was done in the range of 2θ from 2° to 50°. Only the scale factor, background and cell parameters were refined. The molecular positions were optimised by lattice energy minimisation with fixed unit cell parameters between the Rietveld steps.

For one of the pigments (PV23) the quality of the XRPD data was good enough to solve the crystal structure from the powder data. This was done using the Dmol3, X-Cell and Powder Solve modules in Materials Studio [12]. First a geometry optimisation was performed with the gradient-corrected BP potential in the Dmol3 DFT code in Materials Studio. Then the powder diffraction pattern was indexed with the X-Cell indexing program [13] on 18 peaks between 5° and 32° 2θ and an impurity level of 1. The search was performed in the orthorhombic, monoclinic and triclinic crystal systems. Finally, a Reflex Powder Solve run was performed with the above determined unit cell and half of the optimised molecular structure. Ten simulated annealing cycles were applied.

2.1. Pigment Violet 23

Pigment Violet 23 (PV23; also referred to as Carbazole Violet) was patented in 1952 [14] and belongs to the class of dioxazine pigments. It is a commercially important pigment which has a unique blue shade violet color and outstanding resistance to light and weather conditions. PV23 is widely used in various applications including inks, plastics, coatings, textiles and other special purpose media such as contact lenses [15].

PV23 has at least two polymorphs (α, β) as derived on the basis of X-ray powder diffraction data [16], of which only β is commercially important and discussed in this work. The only structural information on this pigment was given in a review article by Hunger [17] showing a figure of the packing of presumably the β polymorph. No information on the α polymorph was found. According to the work [17], the molecule of PV23 is flat and has an inversion center. We assume that flexibility of the ethyl groups does not contribute significantly to the crystal structure. Minimisation of the molecule in the Dreiding force field with ESPD charges leads to significant bending of the molecular plane, therefore a rigid body constraint was applied to keep the molecule flat. However, during minimisation of the structures in the polymorph prediction process, the constraint was relaxed and that did not lead to bending of the molecules. Because intramolecular symmetry is not taken into account during structure generation by the PP, the prediction was performed in the subgroups of the chosen space group containing no inversion symmetry. Since the space group was known ($P2_1/c$, $Z = 2$) from the indexing of the powder pattern, the

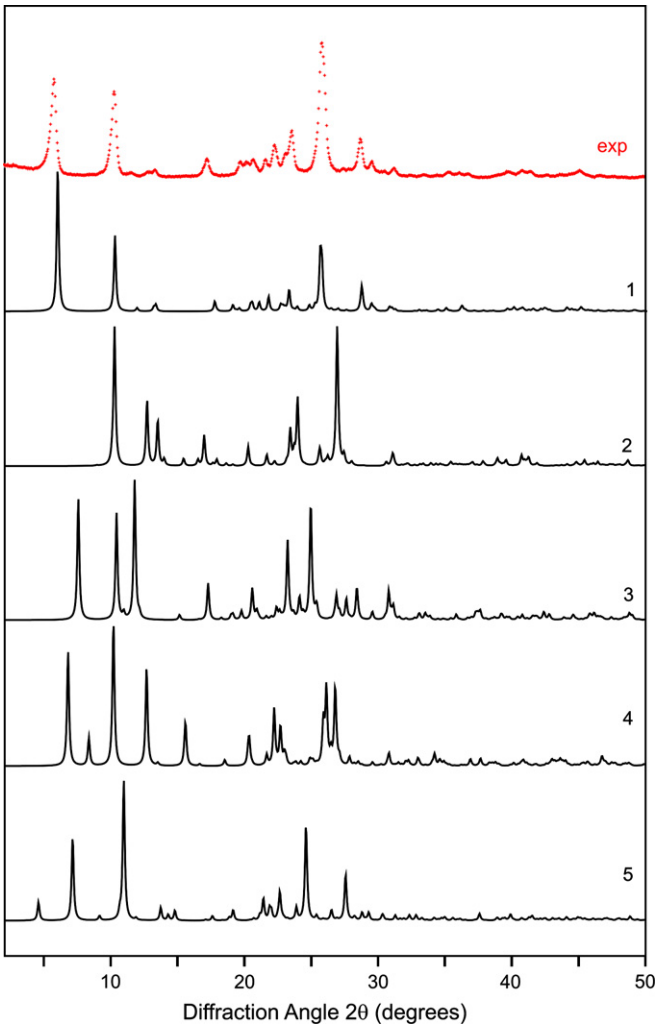

Fig. 2. X-ray powder patterns' comparison of PV23: experimental powder pattern (red) and calculated powder patterns from the first five low energy structures (i.e. without Rietveld refinement). The numbers correspond to the energy ranking of the structure. (For interpretation of the references to color in this figure legend, the reader is referred to the web version of this article.)

search was performed in space group $P2_1$ with one molecule in the asymmetric unit.

The prediction resulted in 69 structures with lattice energies ranging from −299.2 to −181.2 kJ/mol. The structure which fitted the experimental XRPD pattern best was found as number one in the energy ranking, having the lowest energy. The space group was determined to be $P2_1/c$, using the symmetry finder in Cerius[2]. Other structures from the list have significantly different powder patterns so that the chosen structure is without doubt the closest to the real structure of β-PV23 (Fig. 2). In this structure the molecules are packed perpendicular to each other. The low energy of the structure is achieved by an efficient overlap of π-orbitals of the neighbouring molecules along the *b*-axis and Van der Waals forces only (Fig. 3). There are no hydrogen bonds present in the structure as expected for this molecule. The projection of the structure published earlier [17] is in agreement with the structure predicted in the present work. We assume that the structures are similar as no atomic coordinates were available in order to make a proper comparison.

Table 1 gives the crystallographic information about the predicted structure of PV23 and the structure solved from the powder data. Atomic coordinates of both structures can be found in Appendix Tables A1 and A2. Rietveld refinement of the predicted structure converged at an R_p of 20.1% and resulted in a reasonable fit of the powder patterns (Fig. 4).

2.2. Pigment Red 202

Pigment Red 202 (PR202), or 2,9-dichloroquinacridone, belongs to the class of quinacridone pigments. As many of 2,9-substituted derivatives of quinacridone, it shows excellent weather fastness and is widely used for various outdoor applications. PR202 has several polymorphs as known from patents (α, β and γ [18]; platelet [19]). The distinction between the polymorphs mentioned in the patents is based on the difference in peaks in the XRPD pattern, however, the powder data are merely reported in tabular form and can, therefore,

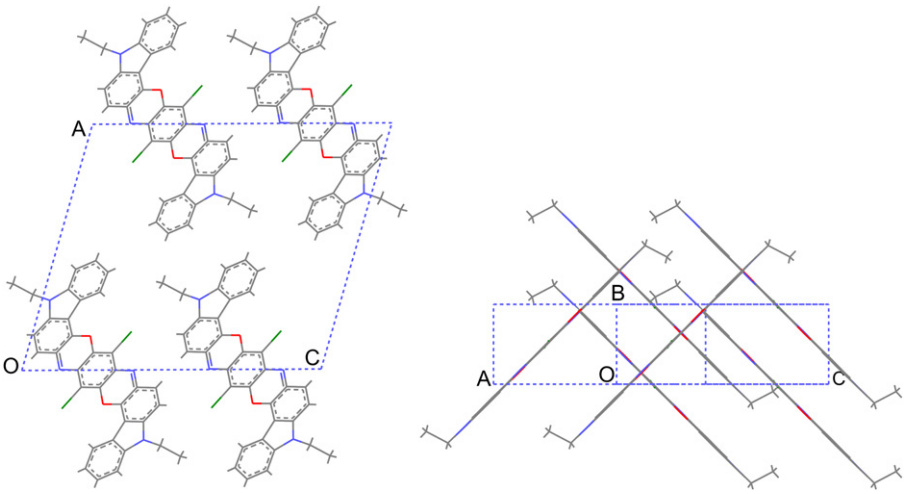

Fig. 3. Predicted crystal structure of Pigment Violet 23. Molecules are nearly perpendicular to each other and are densely packed along the *b*-axis.

Table 1
Crystallographic data of the predicted structure of Pigment Violet 23 as obtained from the Polymorph Predictor and Materials Studio

	Polymorph Predictor		Materials Studio	
	Minimised	Rietveld	Minimised	Rietveld
Space group	$P2_1/c$	$P2_1/c$	$P2_1/c$	$P2_1/c$
Z	2	2	2	2
a (Å)	15.695	15.802	15.606	15.852
b (Å)	4.799	4.649	4.869	4.686
c (Å)	17.955	18.165	17.886	18.232
α (°)	90	90	90	90
β (°)	104.94	104.52	105.97	104.46
γ (°)	90	90	90	90
V (Å^3)	1307	1292	1307	1311
d (g/cm^3)	1.498	1.515	1.498	1.493

Cell parameters are listed for structures before (minimised) and after Rietveld refinement (Rietveld).

Table 2
Crystallographic data and lattice energy (LE) of the first three predicted polymorphs of Pigment Red 202 as obtained from the PP, and assignment to experimental data

Polymorph	#1	#2	MAMGUD01 [20]	#3	#32	MAMGUD [21]
	β	γ	'Red phase'	α		'Black phase'
Space group	$P2_1/c$	P-1	P-1	$P2_1/c$	$P2_1/c$	$P2_1/c$
Z	2	1	1	2	2	2
a (Å)	15.248	6.106	3.782	3.868	4.057	3.782
b (Å)	3.849	3.833	5.831	5.804	15.655	14.840
c (Å)	13.414	16.741	16.754	33.616	12.527	12.942
α (°)	90	94.29	94.96	90	90	90
β (°)	88.88	103.65	95.14	92.14	89.79	91.93
γ (°)	90	94.91	90.66	90	90	90
V (Å^3)	787	378	367	754	796	726
d (g/cm^3)	1.609	1.677	1.727	1.679	1.591	1.744
LE (kJ/mol)	−284.5	−278.2	–	−277.0	−204.2	–

The black phase (assigned to #32) is also mentioned.

not be fully exploited for proper characterisation of the polymorphs. Judging from these data, the γ polymorph is the one which is commercially important and its powder was investigated by us. The positions of peaks in the XRPD patterns of the γ and platelet forms reported are very similar which suggests that they represent the same polymorph.

The structure of a triclinic polymorph of PR202 (space group P-1, $Z = 1$) was recently determined by single crystal X-ray diffraction [20] (reference code MAMGUD01 in the Cambridge Structural Database − CSD) and described by the authors as a red phase. This structure has the same powder pattern as we obtained experimentally and resembles the pattern of γ-PR202 (or the platelet phase) when compared to the information in the patents. Earlier, a structure of another form of PR202 (space group $P2_1/c$, $Z = 2$), a black phase, was determined by the same authors using single crystal X-ray diffraction (reference code MAMGUD in the CSD). Its powder pattern does not correspond to any structure mentioned in the patents.

As the structures of these two polymorphs are known, we limited our search to the subgroups $P1$ and $P2_1$ of P-1 and $P2_1/c$, respectively, with one molecule in the unit cell. This resulted in 37 structures of which two (#2 and #32 in the energy ranking) correspond to the structures MAMGUD01 and MAMGUD, respectively. Table 2 contains the crystallographic details of the structures and Appendix Tables A3–A6 list the atomic coordinates of these structures. Fig. 5 gives the results of the prediction in the form of an energy–density plot. Structure #2 (P-1, $Z = 1$) with a lattice energy of −278.2 kJ/mol is therefore assigned to the γ polymorph of PR202 (Fig. 6). The molecular packing in this crystal structure resembles

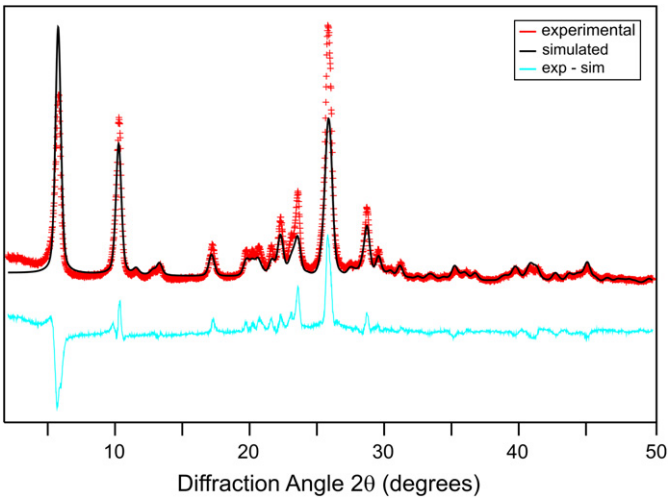

Fig. 4. XRPD pattern of PV23 after Rietveld refinement (black) together with the experimental XRPD pattern (red) and a difference plot (blue). (For interpretation of the references to color in this figure legend, the reader is referred to the web version of this article.)

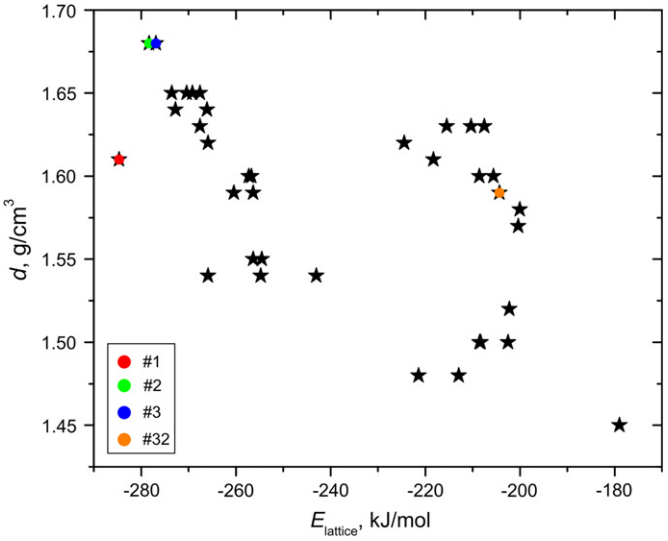

Fig. 5. Results of the polymorph prediction of PR202 as an energy–density plot. Each star represents one structure. Structures of 1, 2, 3, 32 structures in the list of predicted structures are marked with colored signs. (For interpretation of the references to color in this figure legend, the reader is referred to the web version of this article.)

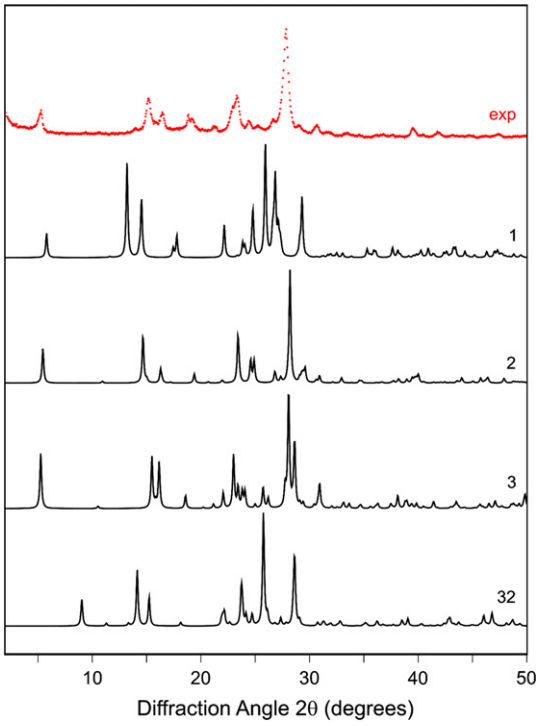

Fig. 6. X-ray powder pattern comparison for PR202: experimental powder pattern (red) and powder patterns of four structures from the prediction. The numbers correspond to the energy ranking of the structures. (For interpretation of the references to color in this figure legend, the reader is referred to the web version of this article.)

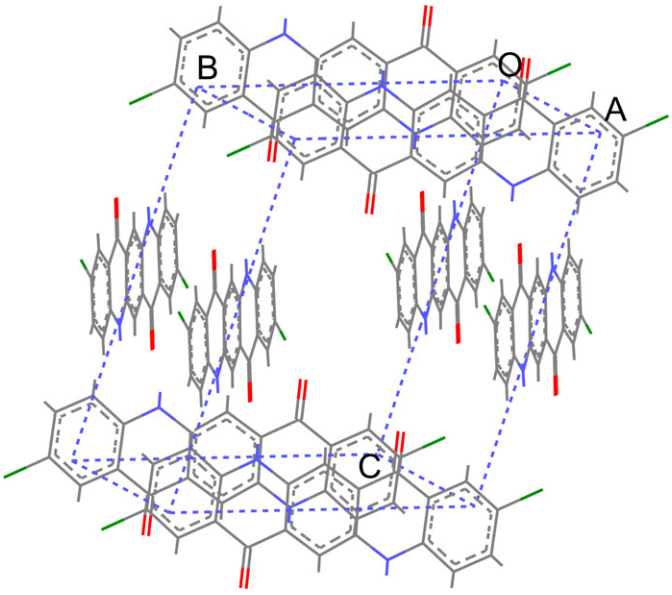

Fig. 8. Structure #32 from the polymorph prediction of Pigment Red 202. This high energy structure contains no H-bonds and is similar to the published structure of the black phase of PR202 (MAMGUD). (For interpretation of the references to color in this figure legend, the reader is referred to the web version of this article.)

that of α-quinacridone (PV19) [8]. Each molecule is connected to two neighbours with four H-bonds forming parallel stacks of molecules in a triclinic structure (see Fig. 7).

The structure of the black phase PR202 is also predicted in the same run by the PP. The projection of the structure is shown in Fig. 8. However, it appears at the end of the list of predicted structures (#32), having a 80.3 kJ/mol higher lattice energy than structure #1. Such a high energy difference is rarely found for metastable polymorphs, making the assignment of the black phase to #32 questionable. We will address this issue further on. The energy of the first three predicted polymorphs in the list differ by only 6.3 kJ/mol in lattice energy, making them possible (metastable) polymorphs.

Since PR202 is chemically very close to the unsubstituted quinacridone (PV19) it can be expected to have similar molecular packings as PV19 which we studied in a previous work [8]. The molecular motif of the structure #1 from the list (space group $P2_1/c$, $Z = 2$) resembles that of γ-quinacridone (PV19) and, therefore, is likely to represent another polymorph of PR202. In this structure each molecule is connected by H-bonds to four neighbours in a criss-cross way (Fig. 9). Its powder pattern indeed corresponds reasonably well to the β form of PR202 from the patent [18], be it that a comparison is limited by the lack of graphical data. The packing of structure #3 from the list (space group $P2_1/c$, $Z = 2$) resembles that of β-quinacridone (PV19) (Fig. 10). This structure can be attributed to the α-PR202 from the patent, but, again, as a result of the lack of detailed powder data in the patent no definite conclusion can be drawn.

Structure #2 was subjected to the Rietveld refinement procedure using our experimental data ($R_p = 26.1\%$) and the resulting XRPD pattern is shown in Fig. 11. Energy minimisation of the MAMGUD01 structure in the force field with the atomic charges used in the prediction indeed resulted in the same structure as was obtained from the PP. This confirms the predicted structure, and at the same time it shows that the high R_p factor of the Rietveld refinement is due to the limited quality of the powder pattern.

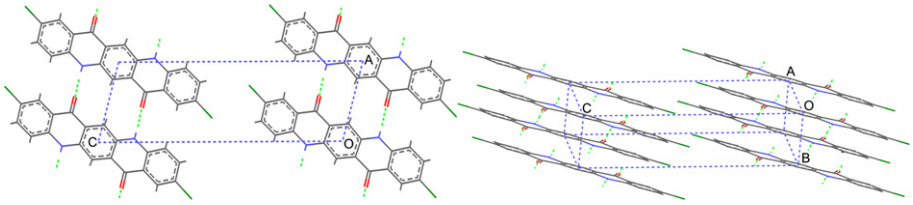

Fig. 7. Structure #2 from the polymorph prediction of Pigment Red 202. The structure corresponds to the γ polymorph of PR202 (MAMGUD01). The molecular packing motif is similar to that of α-quinacridone (Pigment Violet 19).

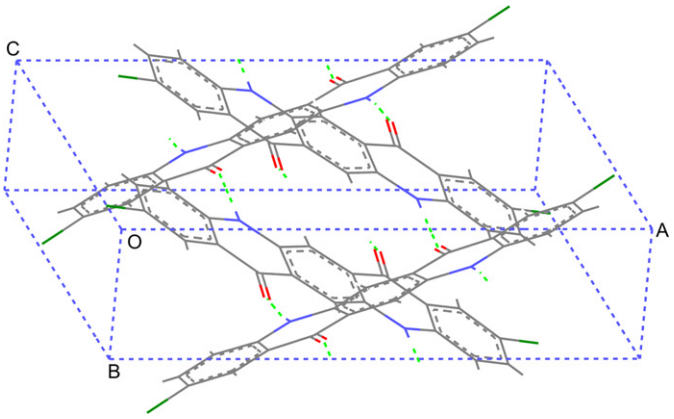

Fig. 9. Structure #1 from the polymorph prediction of Pigment Red 202. This structure corresponds to the β-polymorph of PR202 [18]. The criss-cross molecular motif is similar to that of γ-quinacridone (PV19).

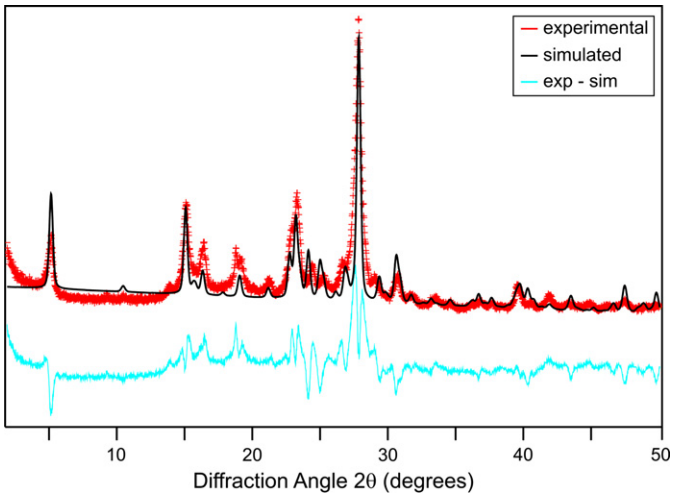

Fig. 11. XRPD pattern of PR202 after Rietveld refinement (black) against the experimental XRPD pattern (red) and a difference plot (blue). (For interpretation of the references to color in this figure legend, the reader is referred to the web version of this article.)

Table 3 summarizes the structural similarities between the polymorphs of PR202 and PV19 based on the space group and typical hydrogen bond motifs in the structures. The polymorph with the criss-cross network of hydrogen bonds (β-PR202 and γ-PV19) is in both cases the most stable one. Metastable polymorphs, however, have a different order of stability, according to the calculated lattice energies of the structures; the triclinic polymorph of PR202 is more stable than the monoclinic one while the opposite result was found for PV19.

2.3. Pigment Yellow 139

Pigment Yellow 139 (PY139) belongs to the class of isoindoline pigments. No information about possible polymorphs was found. The structure of this pigment was solved from the powder data by Erk et al. (FEGDUR in the CSD, [22]). The structure possesses a high symmetry space group *Cmca*, $Z = 8$, which is not among the most common space groups. The molecules, having mirror symmetry themselves, lie on the mirror planes in the structure. Therefore, the prediction was performed in the subgroup $C222_1$ with one molecule in the asymmetric unit.

When the default parameters of the PP for the Monte Carlo step of the generation of structures (4000 trials) were used, none of the resulting structures had a powder pattern similar to the experimental one. The prediction was subsequently performed in five consecutive runs, to produce a total of 10,000 trial structures, and this resulted in 243 structures ranging in lattice energy from −313.8 to −105.0 kJ/mol. The first structure in the energy ranking (space group *Cmca*) produced a powder pattern very close to the experimental one. Rietveld refinement converged at $R_p = 14.5\%$ with a quite convincing difference plot (Fig. 12). Also a minimisation of the energy of the published structure FEGDUR with the force field and atomic charges used for the prediction resulted in the same structure as was obtained by the PP which again indicates the similarity between the predicted and experimental structures. Table 4 gives the crystallographic details of the predicted and published structures. Atomic coordinates are listed in Appendix Table A7.

The predicted structure, as confirmed by the published structure, consists of layers of molecules with a 2D H-bond network (Fig. 13). Some of the donor and acceptor atoms participate in the formation of intramolecular H-bonds.

3. Discussion

PP in combination with XRPD data of limited quality appears to be a very good tool to predict crystal structures of pigments. A rather simple and conventional force field like Dreiding seems to work quite adequately even for highly polarized molecules forming many H-bonds in the structure as in the case of PY139. Nevertheless, the limited quality of the powder diffraction data results in a high R_p factor during

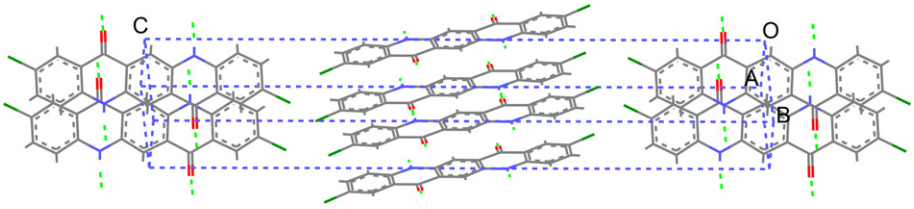

Fig. 10. Structure #3 from the polymorph prediction of Pigment Red 202. This structure corresponds to the α-polymorph of PR202 [18]. The molecular motif is similar to that of β-quinacridone (PV19).

Table 3
Relationship between the polymorphs of PR202 and PV19 on the basis of similarities in H-bond network

	PR202	PV19	
1	β	γ	1
2	γ	α	3
3	α	β	2

Numbers represent the ranking of the stability of the polymorphs according to the calculated lattice energies in the Dreiding force field.

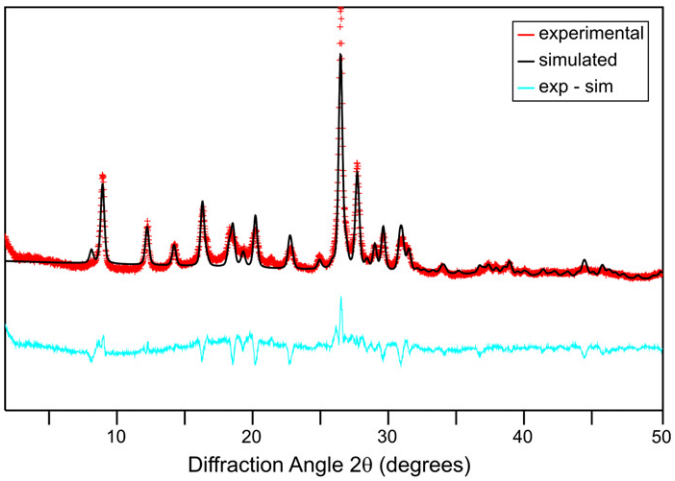

Fig. 12. XRPD pattern of PY139 after Rietveld refinement (black) against the experimental XRPD pattern (red) and a difference plot (blue). (For interpretation of the references to color in this figure legend, the reader is referred to the web version of this article.)

Rietveld refinement and often a fit of limited quality. In most cases the experimental pattern has additional small peaks which do not show up in the calculated pattern. As the sample is not purified before measuring the XRPD pattern, impurities might account for these extra peaks in the pattern which, of course, cannot be fitted during the Rietveld refinement. Also the small particle size typical for pigments causes broadening of the peaks and, therefore, complicates the refinement. Better quality of the powder might improve the resulting structure.

To limit the number of runs for the PP, it is advantageous to have at least some indication of the space groups, involved for

Table 4
Crystallographic data of the predicted structure of Pigment Yellow 139 as obtained from the PP (minimised), after Rietveld refinement (Rietveld) and published data (FEGDUR, [22])

	Minimised	Rietveld	FEGDUR
Space group	*Cmca*	*Cmca*	*Cmca*
Z	8	8	8
a (Å)	20.959	21.159	21.198
b (Å)	6.949	6.830	6.847
c (Å)	18.550	19.301	19.292
α (°)	90	90	90
β (°)	90	90	90
γ (°)	90	90	90
V (Å^3)	2702	2789	2800
d (g/cm^3)	1.806	1.749	1.742

the various polymorphs. If this is not known, one may run the prediction in the space groups most frequently found among organic solids [23]. According to the latter study, 92.7% of all organic crystal structures belongs to 18 space groups. For centrosymmetrical molecules the number of space groups is even smaller, if it is assumed that these molecules crystallise in centrosymmetrical space groups which is very often the case. For example, crystal structure prediction of PV23 and PR202 would be possible even without prior knowledge of the space group, since $P2_1/c$ and P-1 belong to the two most frequent space groups (they account for 36.6% and 16.9% of all organic structures, respectively). Moreover, running the PP in P-1 for $Z = 1$ and $Z = 2$, in principle, generates also structures with higher symmetry as $P2_1/c$, as it contains P-1 as a subgroup. This would demand for a much higher number of trial structures, which is beyond the capacity of the PP in most simulations. Prediction of PY139, however, would not be that successful without prior knowledge of the space group as *Cmca* does not belong to the frequent groups and accounts for only 0.1% of organic crystals.

Since the error of the force field energy calculations is some 5–10 kJ/mol and the structures highest in the list have even smaller differences in energy, the stability order of the calculated structures may not represent the real stability order of the polymorphs. However, the fact that the predicted structures are so close in energy indicates that they are good candidates

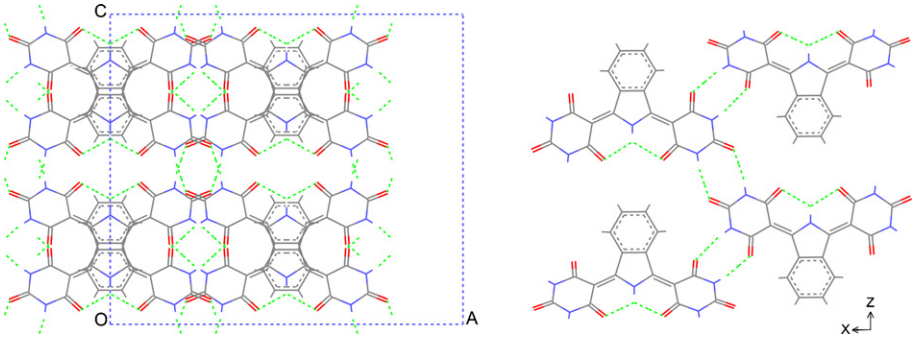

Fig. 13. Predicted crystal structure of PY139. On the right a layer of molecules making up a 2D network of hydrogen bonds (green dotted lines) is shown. (For interpretation of the references to color in this figure legend, the reader is referred to the web version of this article.)

for real polymorphs as experimental polymorphs differ usually not more than 5 kJ/mol in energy [24,25]. In the present study the XRPD data serve as the final assignment tool. This observation, however, makes the structure of the black phase of PR202 doubtful as its lattice energy is about 80 kJ/mol higher than the energy of the stable polymorph. To test the influence of the chosen force field on the stability order of the polymorphs, an alternative, consistent valence force field (CVFF, [26]) was applied to the 4 structures highest in ranking for each pigment. For pigment PV23 this resulted only in the exchange of the second and the third structures, for PY139 this did not lead to any changes in order. Energy minimisation of the PR202 structures from Table 2 leads to a somewhat different stability order of the structures: #2 and #3 (LE = −326.8 and −321.7 kJ/mol, respectively) have lower energy than #1 (−310.9 kJ/mol). The fact that #2 represents now the stable polymorph is interesting, since this structure was experimentally observed. The lattice energy of structure #32 becomes −291.2 kJ/mol which is still 35.6 kJ/mol higher than the energy minimum. Thus, #32 might be regarded as a real polymorph although its lattice energy is still quite high. The impact of the force field on the PP results needs more thorough study which is beyond the scope of the present paper.

4. Conclusions

On the basis of three examples, it has been demonstrated that the PP in combination with powder patterns of limited quality is able to successfully predict the crystal structures of rigid molecules like pigments. This method is reliable as confirmed by experimentally known structures; it gives results consistent with other methods, e.g. indexing of powder data, and it solves the structures of yet unpublished pigments. The crystal structure of PV23, not published earlier, is predicted as first in the list and it matches the experimental powder pattern well. The crystal structure of PR202, predicted as #2 in the list of structures, is in agreement with the published experimental structure. Also a crystal structure of PY139, predicted as #1 in energy ranking, is in good agreement with the published structure. Besides predicting the stable polymorph, the method described also predicts all metastable polymorphs found as well as possible metastable polymorphs, which have not been found yet.

The major advantage of the method is that there is no need for single crystals or powder patterns of high quality. XRPD patterns obtained using standard laboratory based diffractometers are sufficient, even for very fine powders. The resulting structure is perfectly suitable as a starting model for the Rietveld refinement and for any calculation involving force fields for which the crystal structure is essential like morphology prediction [27].

Acknowledgements

This work is supported by the Institute for the Promotion of Innovation by Science and Technology in Flanders (IWT).

Appendix

Table A1
Atomic coordinates of structure #1 of PV23 as obtained from the PP (cf. Table 1)

Atom	*x*	*y*	*z*
C10	−0.07163	−0.18118	0.47282
C11	−0.00043	−0.1762	0.4369
C12	0.07162	0.00542	0.46412
C13	−0.07189	−0.52417	0.34836
C14	−0.14321	−0.53403	0.38355
C15	−0.21297	−0.72092	0.35402
C16	−0.21367	−0.89176	0.29085
C17	−0.14337	−0.88018	0.25564
C18	−0.07232	−0.69619	0.28487
N20	−0.00354	−0.34894	0.37646
O22	0.14014	0.36127	0.55538
Cl24	−0.15713	−0.01782	0.57749
H27	−0.14317	−1.00316	0.2092
H28	−0.02070	−0.68649	0.26015
C36	−0.28969	−0.78124	0.37544
C37	−0.33413	−0.98639	0.32444
C38	−0.41542	−1.09087	0.33197
C39	−0.45012	−0.98782	0.39167
C40	−0.40500	−0.77990	0.44227
C41	−0.32393	−0.67382	0.43458
N42	−0.28735	−1.05005	0.27299
H47	−0.44877	−1.24013	0.29544
H48	−0.50837	−1.06405	0.39852
H49	−0.43141	−0.70567	0.48479
H50	−0.29097	−0.52300	0.47098
C53	−0.31015	−1.24643	0.21072
C54	−0.34852	−1.10045	0.13281
H60	−0.25195	−1.36469	0.20748
H61	−0.35816	−1.39822	0.21994
H62	−0.36138	−1.25339	0.08626
H63	−0.41026	−0.99792	0.13344
H64	−0.30266	−0.94512	0.12155

Table A2
Atomic coordinates of the PV23 structure as obtained by material studio from the XRPD (cf. Table 1)

Atom	*x*	*y*	*z*
C1	0.07133	1.49080	−0.53600
C2	0.00041	1.32573	−0.43655
C3	0.07131	1.31718	−0.47269
O4	0.13970	1.13589	−0.44440
C5	0.14282	0.96540	−0.38312
C6	0.07160	0.97978	−0.34795
N7	0.00321	1.15569	−0.37591
C8	0.07225	0.81126	−0.28398
C9	0.14309	0.62489	−0.25462
C10	0.21326	0.60838	−0.28993
C11	0.21267	0.77756	−0.35322
C12	0.28933	0.71402	−0.37441
C13	0.33353	0.50833	−0.32345
N14	0.28674	0.44708	−0.27199
C15	0.41480	0.40178	−0.33096
C16	0.44972	0.50348	−0.39045
C17	0.40463	0.71170	−0.44105
C18	0.32366	0.81973	−0.43339
C19	0.30908	0.24969	−0.21013
C20	0.35054	0.39457	−0.13207
Cl21	0.15640	1.47452	−0.57781

Table A2 (*continued*)

Atom	*x*	*y*	*z*
H22	0.02071	0.82520	−0.25930
H23	0.14290	0.50296	−0.20811
H24	0.44781	0.25203	−0.29430
H25	0.50810	0.42630	−0.39708
H26	0.43091	0.78526	−0.48354
H27	0.29069	0.97105	−0.46964
H28	0.35584	0.09598	−0.21983
H29	0.24962	0.13766	−0.20688
H30	0.30583	0.55282	−0.12135
H31	0.41346	0.48893	−0.13314
H32	0.36286	0.24578	−0.08468

Table A3
Atomic coordinates of structure #1 of PR202 as obtained from the PP

Atom	*x*	*y*	*z*
C14	−0.42401	0.16025	0.46029
C15	−0.42865	0.07717	0.56272
C16	−0.50581	−0.08433	0.60214
H22	−0.51085	−0.14655	0.67625
N23	−0.35243	0.31362	0.42081
C24	−0.28264	0.40113	0.47382
C25	−0.28042	0.33198	0.57642
C26	−0.35411	0.16416	0.61843
C27	−0.21245	0.56433	0.42467
C28	−0.13835	0.66465	0.47851
C29	−0.13516	0.59906	0.58163
C30	−0.20588	0.43191	0.63068
O31	−0.35278	0.08578	0.70914
H32	−0.35091	0.36294	0.35037
H33	−0.21489	0.61276	0.34999
H34	−0.08707	0.78677	0.44278
Cl35	−0.04695	0.72339	0.64720
H36	−0.202567	0.38464	0.70575

Table A4
Atomic coordinates of structure #2 of PR202 as obtained from the PP

Atom	*x*	*y*	*z*
C14	0.01469	−0.12438	0.07591
C15	0.19212	0.04922	0.06859
C16	0.20459	−0.17056	0.00863
H22	0.35236	−0.29008	0.01638
N23	0.03363	−0.25067	0.14693
C24	0.13696	−0.21357	0.21465
C25	0.35105	−0.05043	0.21390
C26	0.37246	0.08782	0.14036
C27	0.09740	−0.34549	0.28594
C28	0.27433	−0.32685	0.35771
C29	0.49215	−0.17570	0.35717
C30	0.52994	−0.03623	0.28562
O31	0.55729	0.25907	0.13980
H32	0.17553	−0.38011	0.14887
H33	0.05951	−0.45555	0.28615
H34	0.24490	−0.42524	0.40985
Cl35	0.70945	−0.16333	0.44173
H36	0.68870	0.07269	0.28620

Table A5
Atomic coordinates of structure #3 of PR202 as obtained from the PP

Atom	*x*	*y*	*z*
C14	0.87448	0.07449	0.46225
C15	1.05652	−0.13601	0.46562
C16	1.17978	−0.20931	0.50397
H22	1.30860	−0.36125	0.50744
N23	0.74768	0.14977	0.42687
C24	0.79198	0.03489	0.39299
C25	0.96485	−0.17772	0.39294
C26	1.10276	−0.25728	0.42972
C27	0.65873	0.13090	0.35761
C28	0.68792	0.01308	0.32134
C29	0.84984	−0.20381	0.32096
C30	0.99015	−0.29772	0.35659
O31	1.28044	−0.43925	0.43006
H32	0.61671	0.29236	0.42589
H33	0.53953	0.28623	0.35798
H34	0.58952	0.08406	0.29542
Cl35	0.87583	−0.35323	0.27801
H36	1.10855	−0.45429	0.35575

Table A6
Atomic coordinates of structure #32 of PR202 as obtained from the PP

Atom	*x*	*y*	*z*
C14	2.18794	0.06774	0.54262
C15	2.06528	0.07343	0.43753
C16	1.87666	0.00479	0.39513
H22	1.78655	0.00831	0.31895
N23	2.36869	0.13118	0.58473
C24	2.43487	0.20364	0.53208
C25	2.32270	0.21615	0.42758
C26	2.14105	0.14936	0.38186
C27	2.62020	0.26633	0.58319
C28	2.69459	0.34353	0.53071
C29	2.58321	0.35700	0.42564
C30	2.39500	0.29361	0.37460
O31	2.03842	0.15855	0.28845
H32	2.45562	0.12473	0.65555
H33	2.70246	0.25703	0.65894
H34	2.83065	0.38945	0.56885
Cl35	2.67595	0.44828	0.35967
H36	2.30957	0.30414	0.29904

Table A7
Atomic coordinates of the PY139 structure as obtained from the PP

Atom	*x*	*y*	*z*
C2	0.53345	−0.93044	−0.26045
C5	0.46653	−0.91474	−0.39174
C6	0.43277	−0.91817	−0.32633
N8	0.50000	−0.92015	−0.14889
C9	0.55326	−0.92870	−0.18808
C16	0.38649	−0.92682	−0.15621
C17	0.37502	−0.85772	−0.08782
N18	0.31800	−0.83153	−0.06150
C19	0.26868	−0.88079	−0.09876
N20	0.27448	−0.96219	−0.16096
C21	0.33104	−0.98879	−0.18800
O25	0.32762	−1.08475	−0.24402
O26	0.21500	−0.84816	−0.07458
O27	0.41697	−0.80596	−0.04536
H30	0.44237	−0.91048	−0.43955
H31	0.38446	−0.90682	−0.32865
H32	0.50000	−0.90827	−0.09658
H35	0.31267	−0.77319	−0.01589
H36	0.23830	−1.00228	−0.18705

References

[1] Smith HM. High performance pigments. Weinheim: Wiley-VCH; 2001.
[2] Christie RM, Hill JM, Rosair G. Dyes Pigments 2006;71:194–8.
[3] Lommerse JPM, Motherwell WDS, Ammon HL, Dunitz JD, Gavezzotti A, Hofmann DWM, et al. Acta Crystallogr Sect B Struct Sci 2000;56:697–714.
[4] Motherwell WDS, Ammon HL, Dunitz JD, Dzyabchenko A, Erk P, Gavezzotti A, et al. Acta Crystallogr Sect B Struct Sci 2002;58:647–61.
[5] Day GM, Motherwell WDS, Ammon HL, Boerrigter SXM, Della Valle RG, Venuti E, et al. Acta Crystallogr Sect B Struct Sci 2005;61:511–27.
[6] Erk P. In: Smith HM, editor. High performance pigments. Weinheim: Wiley-VCH; 2001. p. 103–23.
[7] Schmidt MU, Ermrich M, Dinnebier RE. Acta Crystallogr Sect B Struct Sci 2005;61:37–45.
[8] Panina N, Leusen FJJ, Janssen FFBJ, Verwer P, Meekes H, Vlieg E, et al. J Appl Crystallogr 2007;40:105–14.
[9] Cerius2, v.4.71. Accelrys Software Inc.; 2002.
[10] Frisch MJ, Trucks GW, Schlegel HB, Gill PMW, Johnson BG, Robb MA, et al. Gaussian 94 (Revision D.4). Pittsburgh, PA: Gaussian Inc.; 1998.
[11] Wiles DB, Young RA. J Appl Crystallogr 1981;14:149–51.
[12] Materials Studio, v.4.0. Accelrys Software Inc.; 2005.
[13] Neumann MA. J Appl Crystallogr 2003;36:356–65.
[14] Hoechst. DE-PS Patent 946,560; 1952.
[15] Chamberlain T. In: Smith HM, editor. High performance pigments. Weinheim: Wiley-VCH; 2001. p. 185–94.
[16] Nicolaou C. In: Smith HM, editor. High performance pigments. Weinheim: Wiley-VCH; 2001. p. 333–62.
[17] Hunger K. Rev Prog Color 1999;29:71–84.
[18] Deuschel W, Honigmann B, Jettmar W, Schroeder H. US Patent 3,157,659; 1963.
[19] Baebler F, Jaffe EE. Eur Patent 0466649A1; 1992.
[20] Senju T, Nishimura N, Hoki T, Mizuguchi J. Acta Crystallogr Sect E Struct Rep Online 2005;61:O2596–8.
[21] Senju T, Hoki T, Mizuguchi J. Acta Crystallogr Sect E Struct Rep Online 2005;61:O1061–3.
[22] Erk P, Hengelsberg H, Haddow MF, van Gelder R. Cryst Eng Commun 2004;6:474–83.
[23] Baur WH, Kassner D. Acta Crystallogr Sect B Struct Sci 1992;48:356–69.
[24] Burger A, Ramberger R. Mikrochim Acta 1979;II:273–316.
[25] Burger A, Ramberger R. Mikrochim Acta 1979;II:259–71.
[26] Lifson S, Hagler AT, Dauber P. J Am Chem Soc 1979;101:5111–21.
[27] Panina N, van de Ven R, Janssen FFBJ, Meekes H, Vlieg E, Deroover G, in preparation.